Journal of The Electrochemical Society, **160** (8) A1031-A1038 (2013)
0013-4651/2013/160(8)/A1031/8/$31.00 © The Electrochemical Society

Expansion of Lithium Ion Pouch Cell Batteries: Observations from Neutron Imaging

Jason B. Siegel,[a,*,z] Anna G. Stefanopoulou,[a] Patrick Hagans,[b] Yi Ding,[c,*] and David Gorsich[c]

[a]*Department of Mechanical Engineering, University of Michigan, Ann Arbor, Michigan 48109, USA*
[b]*Navitas Systems ASG, Ann Arbor, Michigan 48108, USA*
[c]*U.S. Army Tank Automotive Research, Development and Engineering Center (TARDEC), Warren, Michigan 48397-5000, USA*

The expansion of battery material during lithium intercalation is a concern for the cycle life and performance of lithium ion batteries. In this paper, electrode expansion is quantified from in situ neutron images taken during cycling of pouch cells with lithium iron phosphate positive and graphite negative electrodes. Apart from confirming the overall expansion as a function of state of charge and the correlation with graphite transitions that have been observed in previous dilatometer experiments we show the spatial distribution of the expansion along the individual electrodes of the pouch cell. The experiments were performed on two cells with different electrode areas during low and high c-rate operation. The measurements show how charging straightened the cell layers that were slightly curved by handling of the pouch cell during setup of the experiment. Subsequent high charging rate, that exceeded the suggested operating voltage limits, was shown to have a strong influence on the observed expansion. Specifically, during high-rate cycling, the battery showed a much larger and irreversible expansion of around 1.5% which was correlated with a 4% loss in capacity over 21 cycles.
 [DOI: 10.1149/2.011308jes]

Manuscript submitted February 1, 2013; revised manuscript received April 15, 2013. Published April 27, 2013. This was Paper 506 presented at the Seattle, Washington, Meeting of the Society, May 6–10, 2012.

Expansion and contraction of battery material during charging and discharging can lead to fracture of the electrode and eventually capacity loss as particles are no longer electrically connected to the current collector, each other, or the carbon matrix in which they are suspended. The carbon anode material is known to expand upon intercalation of lithium into the host structure that occurs during charging of the battery. Expansion of the graphite can cause deformations as large as 10% of the anode volume[1,2] depending upon the type of carbon. The stress that develops inside the battery is also related to the rate of charging.[3]

Lee et al.[4] measured the dimensional changes in lithium cobalt oxide pouch cells during cycling using a specialized dilatometer setup. They found that the expansion of the battery consists of two components: an irreversible thickness increase, corresponding to initial formation of the solid electrolyte interface (SEI), and one which is reversible and follows the battery state of charge, expanding upon charging.[4] They attributed the volume change during cycling, approximately 2% of the total battery initial thickness, to the anode active material since the cobalt oxide does not show significant volume change upon lithium intercalation.

In this paper we document the expansion of Lithium Iron Phosphate ($LiFePO_4$ or LFP) pouch cells upon charging. The measurements are taken using Neutron Imaging (NI), an in situ technique similar to X-ray imaging that is sensitive to lighter elements such as hydrogen and lithium. We also provide a method for quantifying the expansion from the NI data. We observed a 0.5% total cell expansion (after SEI formation), which corresponds to a 1.7% expansion of the graphite material if attributed entirely to the negative electrode active material and ignoring the potential contraction of the positive electrode.[5,6] The impact of charging rate was also investigated by applying a 5C charge-discharge cycle to the battery with an increased voltage window. A non-recoverable increase in the battery thickness from cycle to cycle was observed under this abusive condition, which was correlated with a 4% decrease in capacity throughout the test.

Experimental

The neutron imaging was performed at the National Institute for Standards and Technology (NIST) Center for Neutron Research. The collimated neutron beam originates from a 20 MW reactor, which provides the high flux source of neutrons. The transmission image is captured by a micro-channel plate (MCP) neutron counting detector with 5 μm pixel pitch and 13.5 μm spatial resolution. Further details about the detector and facility can be found in.[7,8] The battery pouch is mounted on a fixture in front of the detector so that the neutron beam path, which travels into the page along the z-axis, is parallel to the plane of the separator as shown in Figure 1. The resulting images formed on the detector are a two-dimensional projection of the battery structure onto the detector surface.

Two battery pouch cells were used for the experiment. The designs of the batteries are similar each having a stacked electrode structure and the only difference was the electrode areas as shown in Table I. The batteries consisted of 11 double sided negative electrodes and 10 positive electrodes stacked inside the pouch and electrically connected in parallel. The batteries were then filled with electrolyte, sealed, formed (cycled) and finally re-sealed in a glove box. The $LiFePO_4$ active material is 54 μm thick applied to each side of a 20 μm aluminum current collector, yielding a total thickness of 128 μm for the positive

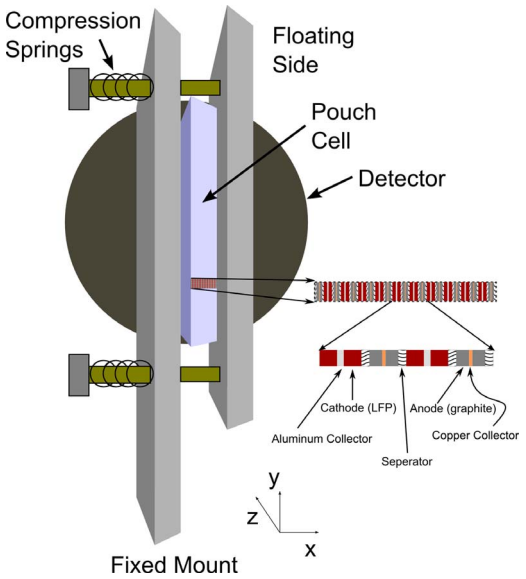

Figure 1. The Battery pouch cell is positioned in front of the neutron sensitive detector so that the beam axis (z-direction) is parallel to the separator. The inset drawing shows a cross-section of the layered battery structure.

*Electrochemical Society Active Member.
[z]E-mail: siegeljb@umich.edu

Table I. Electrode Dimensions.

	Anode	Cathode
Active Material (Thickness)	39 μm carbon	54 μm LiFePO4
Current Collector (Thickness)	10 μm copper foil	20 μm aluminum foil
Sample A (Active Area)	15 mm × 25 mm	13 mm × 25 mm
Sample B (Active Area)	7 mm × 45 mm	5 mm × 45 mm

electrode. The carbon active material is 39 μm thick applied to each side of a 10 μm copper current collector, yielding a total thickness of 88 μm for the negative electrode. The separator is 25 μm thick. All of the dimensions are summarized in Table I.

The first battery, (sample A) is a standard size 120 mAh cell used in.[7] This battery had a width of approximately 1.5 cm and height of 2.5 cm. The 2nd battery (sample B) is also a 10-layer pouch cell constructed from strips cut from A123 production Plug in Hybrid Electric Vehicle (PHEV) electrode material. The battery dimensions used for sample B, listed in Table I, were chosen to maximize the utilization of the available detector area and optimize the neutron transmission through the sample as described in,[7] resulting in the tall narrow cell design. The negative electrode strip is 7 mm wide carbon on a copper foil and the positive electrode is 5 mm wide $LiFePO_4$ on an aluminum collector. The electrodes were hand stacked with a woven separator and banded together using Kapton tape around the middle to hold the electrodes in place before inserting into the pouch. The measured capacity of this battery was 64 mAh.

Since sample B was hand stacked, it was first imaged using X-ray tomography to ensure the flatness of the layers. Flatness of the battery layers and alignment parallel to the neutron beam path are critical to achieve high quality data sets. If the layers are not flat or not parallel to the beam axis then the resulting images will be blurred because they are a projection through multiple layers of the battery. The copper current collectors of the negative electrode correspond to the very bright regions in the slice from the X-ray tomographic image shown in Figure 2. The 1/8″ thick Teflon block visible on the right side of the image was placed inside the pouch cell to help maintain rigidity and flatness of the electrode layers. The metal foil pouch surrounding the battery is also well resolved in the X-ray image.

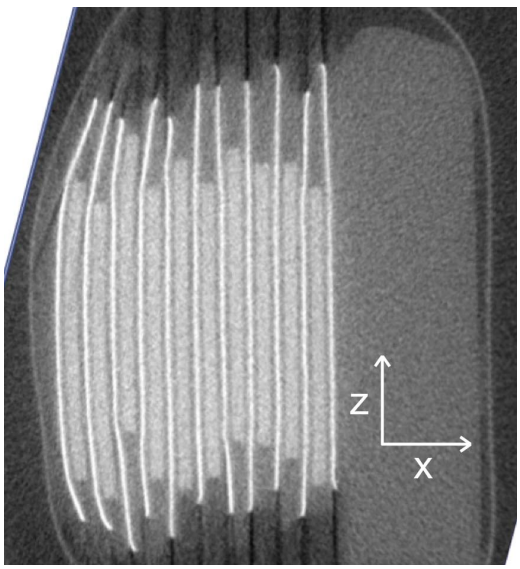

Figure 2. A horizontal slice of the battery (x-z plane) from X-ray tomography is used to observe the flatness of the battery layers. The 11 bright layers in the X-ray image correspond to the copper current collectors of the negative electrodes. A Teflon block was placed inside the pouch cell, shown on the right side of the image, to help maintain rigidity of the battery and keep the electrodes straight. Flatness is important because the neutron images are projections of the structure along the z-axis onto the x-y plane of the detector.

The orientation of the sample as mounted in the neutron beam is shown in Figure 1. Sample A was taped onto an aluminum block which provided a mounting surface, but no external force was applied; therefore the battery was free to swell during charging. Sample B was placed into a fixture that applied pressure on the surface of the pouch cell using a spring loaded mechanism. The two springs, each having a spring rate of 10.86 lbs. per inch, applied a nominal pressure of 3 lbs. over an area of 0.49 square inches (7 mm wide × 45 mm tall). This yielded an actual pressure of approximately 12 psi (82.7 kpa). Since the clamping force is applied via springs the battery is able to deform during cycling if the spring force is overcome. The clamping fixture with springs is shown in Figure 1. The aluminum plate on the left is mounted to a fixed optical table, while the plate on the right is spring loaded and free to move as the battery thickness changes. High compression or rigid fixture of the battery compression plates could contribute to closure of the membrane pores during charging.[9] However because of the low pressure applied by the spring loaded fixture used we do not anticipate any seperator creep in our experiments.

Principle of Neutron Imaging

Neutron transmission imaging is similar to X-ray imaging. The neutron sensitive detector, placed behind the object of interest, measures the transmitted neutron beam intensity by localizing and counting the number of neutrons which hit the surface of the detector over a given time period. The neutron beam intensity after passing through an object of thickness δ can be described by the Lambert-Beer Law;

$$I(t) = I_0 \exp\left(-N_A \delta \left(\sigma_{Li} c_{Li}(t) + \sum \sigma_i c_i\right)\right) \quad [1]$$

where I_0 is the incident neutron beam intensity, σ_{Li} is the neutron cross section (cm^2) of lithium, the σ_i's are the cross section of each other materials in the battery, N_A is Avogadro's number, $c_{Li}(t)$ is the time varying concentration of lithium (mol cm^{-3}), and the remaining c_i's are the concentrations of each of the other materials in the sample that are assumed to be invariant during charging and discharging. Lithium and hydrogen have large neutron cross sections, so these elements strongly attenuate the beam, relative to other materials present in the battery. Therefore, areas of the battery with a high density of lithium atoms, for example the negative electrode layer of a charged battery, will allow the transmission of fewer neutrons. Specifically, changes in the observed intensity during charging and discharging were used earlier in[7] to visualize and quantify the spatiotemporal changes in lithium concentration across the electrode. In this paper the expansion of each of the 10 layers of the two pouch cells is observed by tracking the location of the aluminum current collectors.

The ability to accurately locate edges in the image, and to detect small changes in lithium concentration, is limited by the image exposure time and the detector spatial resolution. Since the measurement noise is governed by neutron counting, which can be modeled as a Poisson random process, a relationship between the measurement uncertainty and image exposure time can be determined.[7] Based on this analysis we find that at least 20 minutes of exposure time is required for each measurement to achieve a good Signal to Noise Ratio (SNR). Another significant challenge is that the spatial resolution of the detector is 13.5 μm, which is larger than the expected per layer expansion of the electrode. Therefore special experimental and image processing techniques were developed to achieve sub-pixel resolution of the expansion at high c-rates. Spatial averaging of the images combined with stroboscopic time averaging of periodic cycles are used to enhance the SNR during charge-discharge experiments at various c-rates. Finally techniques to address the challenges of extracting quantitative data about the expansion of the battery layers from the neutron images will be presented.

Stroboscopic imaging for measurement during high C-rate.— Temporal averaging of subsequent images can be used to increase the neutron counting rate, which increases the signal to noise ratio.

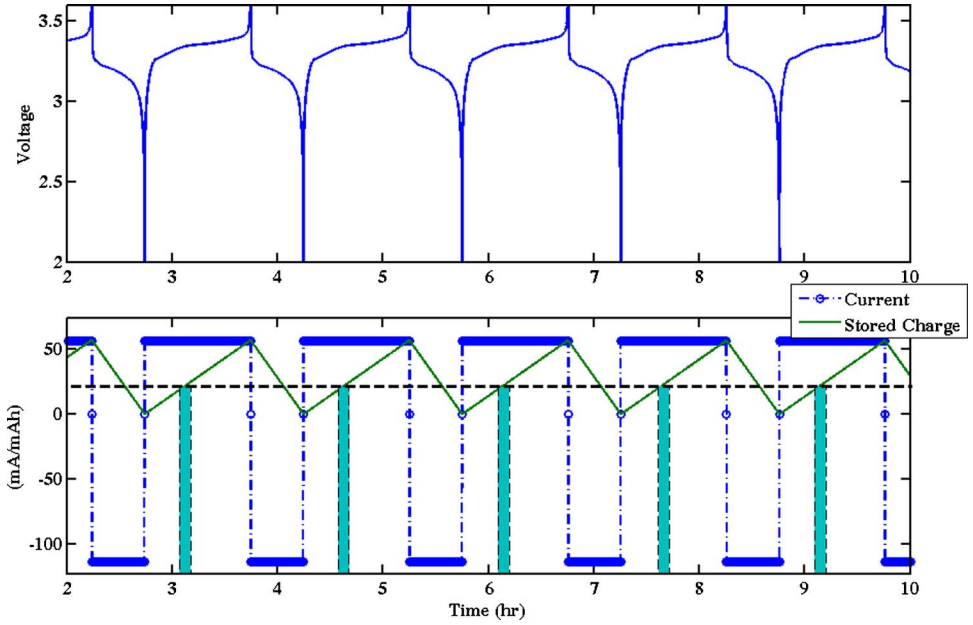

Figure 3. Stroboscopic 1C charge and 2C discharge profile applied to Sample B. The battery was cycled at constant current between 2 V and 3.6 V. Imaging was triggered at the same point in time during the discharge curve and averaged over multiple cycles to increase the effective exposure time.

However, the 20 minute exposure time needed to get good quality data would prevent imaging of high C-rate charging and discharging. Therefore a stroboscopic imaging technique is applied to study transients. A periodic current profile is applied to the battery, as shown in Figure 3, and image acquisition is synchronized with the start of each cycle. Therefore, each image during the charge or discharge period can be acquired with relatively fast (20–45 s) exposure time to allow testing high c-rates and multiple frames from subsequent cycles can be averaged together to achieve the desired SNR.

Line profiles.— Spatial averaging over a uniform region in the image is another way to increase the number of counted neutrons, and hence decrease the measurement uncertainty without requiring excessively long exposure times.[8] Due to the planar structure of the electrode and its aspect ratio it is expected to see swelling along the *x*-direction due to lithium intercalation in the electrode material. Given the X-ray image of the structure in Figure 2, even for the hand-stacked battery, it is reasonable to assume that the structure in the y and z-axis is uniform. Hence, the two-dimensional image data can be averaged along the y-axis without loss of information. This yields the same reduction in noise and an N fold increase in the neutron count rate, where N = 4000 is the number of averaged pixels in the image. Averaging along the y-direction reduces the data to a line profile as shown in Figure 4.

The metal anode and cathode current collectors should produce high contrast edges in the image due to the larger difference in

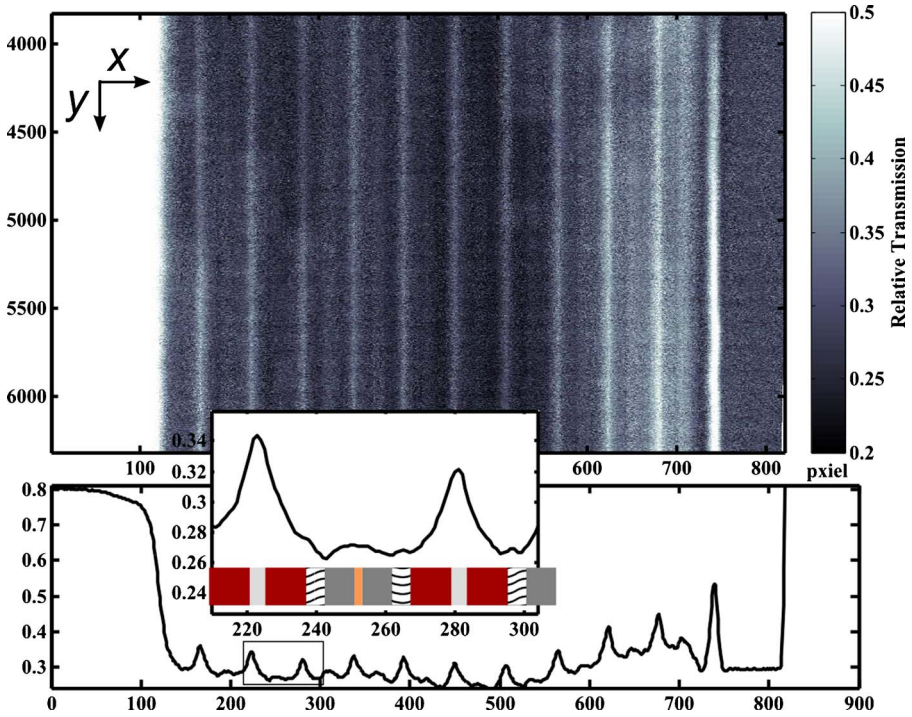

Figure 4. The upper subfigure shows a neutron transmission image of the battery. The lower subfigure shows the corresponding line profile from averaging along the y-axis in the image. The bright streaks in the image that correspond to the peaks in the line profile are caused by the aluminum current collectors which have significantly lower neutron attenuation than other materials present in the battery.

neutron transmission relative to the surrounding active material. The peaks in the line profile are caused by the aluminum current collectors which have significantly lower neutron attenuation ($N_A\sigma_{Al}c_{Al} = 0.094\,\mathrm{cm}^{-1}$) than other materials present in the battery. The copper current collector also has low neutron attenuation ($N_A\sigma_{Cu}c_{Cu} = 0.9\,\mathrm{cm}^{-1}$), but is thinner and therefore cannot be clearly resolved. The Cu sheet could have been more visible (higher peaks) if they were thicker, however 10 μm is narrower than the detector spatial resolution as opposed to the 20 μm thickness of the aluminum foil. The electrolyte soaked polypropylene separator has the largest attenuation ($N_A\sigma_{pp}c_{pp} = 4.23\ \mathrm{cm}^{-1}$). The lowest intensity is expected in the region where the separators are located as they contain a high density of hydrogen atoms which strongly attenuates the neutron beam. However, the thin membrane separator and its proximity to the electrodes which have a similar neutron attenuation (2.4–3.6 cm^{-1}) does not allow us to distinguish clearly its location. The inability to distinguish the separator from the electrode unfortunately limits us from distinguishing the real anode expansion and cathode contraction during charging. Instead the total cell expansion, which is the composite of a potential anode expansion and cathode contraction, can only be quantified.

Quantifying expansion.— Although the movement of the aluminum peak between images of the battery in the charged and discharged state is clearly visible to the human eye, a method to accurately quantify the expansion from the line profile data is needed. Expansion of the battery layers can be quantified by tracking the movement of the 10 peaks in the line profile. However, due to the detector spatial resolution the edges from the aluminum are blurred in the images. Therefore we model the resulting blurred edges of each thin layer using a Gaussian function. The peaks in the line profile are fit with a symmetric function,

$$f(x,a) = a_1 \exp[-a_2(x-a_3)^2] + a_4 \exp[-a_5|x-a_3|] + a_6, \qquad [2]$$

in order to locate the center of the peak, which is defined by the variable a_3. The parameters a_1-a_6 are identified using a nonlinear least squares curve fitting algorithm,

$$\min_a \|f(x,a) - data\|_2\,, \qquad [3]$$

which is based on the interior-reflective Newton method.[10] The algorithm seeks to minimize the two norm of the error between the model and the intensity data from the line profile using 25 data points on each side of the peak as shown in Figure 5.

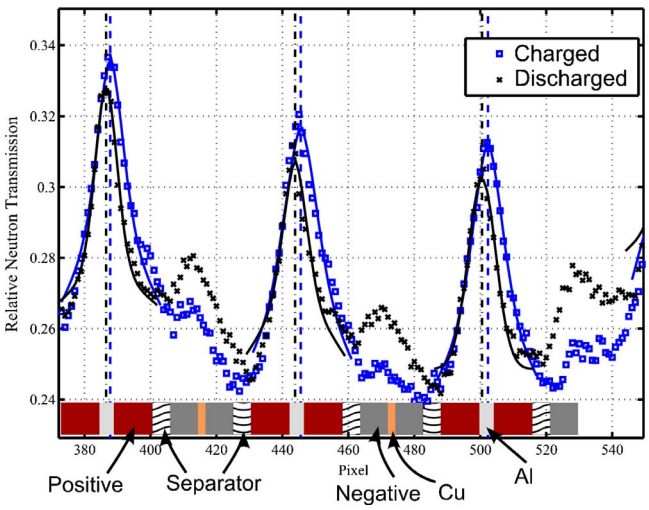

Figure 5. Fitting the peaks in the line profile data which correspond to the aluminum current collectors. The cell fixture is mounted on the left, so expansion of each layer causes compounded displacement of each layer moving rightward.

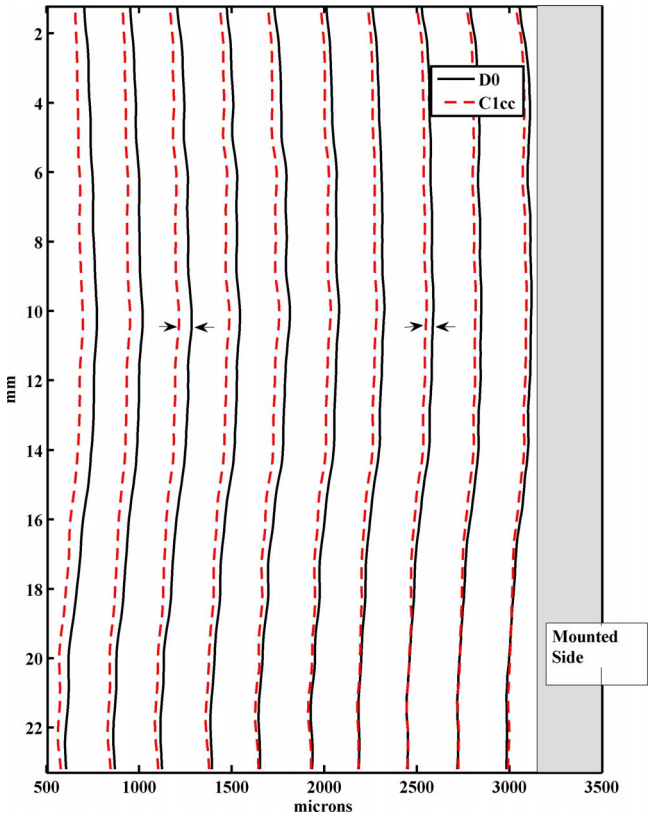

Figure 6. Fit locations of the 10 peaks corresponding to the aluminum layers at the beginning and end of the experiment for sample A, before and after charging the battery. The largest swelling occurred in the middle of the cell. Notice the displacements increase from right to left since the battery was free to expand in this direction.

Using this methodology a sub pixel expansion of the battery layers can be detected by fitting the blurred edge in the image,[11] despite the coarse resolution of the neutron sensitive detector relative to the layer thickness. After processing the data, the average of the 10 cells' peak spacing matched the expected peak spacing of 265 μm based on the nominal values of the materials used in construction.

The center of each peak is indicated by a vertical line as in shown in Figure 5. The expansion of the battery layers during charging results in a shift of each layer to the right since the battery is rigidly mounted on the left side for sample B. Sample A is mounted on the right side as shown in Figure 6. The swelling of each stacked electrode compounds the displacement of the outermost layer. Therefore a small expansion of each layer can be measured by the larger displacement of the outer layer. The quantification of the average total displacement along the y-direction divided by the number of cells provides a more reliable measurement of the expansion, and is used from now in this paper.

The advantage of using NI to measure the thickness of the battery, as compared to a traditional dilatometer, is that multiple points along the electrode (y-axis of the image) can be visualized to study the cell construction and non-uniformity along the surface of the electrode as shown in Figure 6. The layer to layer variability across the x-direction, within the pouch cell, could also be investigated using the NI technique as the expansion of each individual layer in the stacked electrode structure can be measured. Gassing at the anode, due to formation of new Solid Electrolyte Interface (SEI) layer on freshly exposed carbon due to particle fracture,[3] or at the cathode due to electrolyte breakdown under high potentials can also lead to expansion of the battery. A dilatometer would not be able to discern the differences between electrode expansion and displacement due to formation of gasses, however if the gas pocket is large enough NI may be able to detect these differences due to the large change in density and transmission through the sample.

Table II. Summary of experimental conditions.

Sample	**A: Thumb sized Cell** Area: 2.5 cm × 1.5 cm Capacity: 120 mAh No Compression	**B: Skinny Cell** Area: 4.5 cm × 0.5 cm Capacity: 68 mAh 12 PSI Compression Fixture
Experiment	A1: C/5 with rests (1 cycle) A2: 5C cycling over Voltage Window 2–4 V (no rest, stroboscopic)	B1: 1C/2C cycling over voltage window 2–3.6 V (no rest, stroboscopic) B2: 1C charge CC-CV followed by 5C discharge for 6 min, rest for 6 min, and 5C discharge for 6 min to reach 2 V (stroboscopic)
Result	Low-rate cycling showed expected results as compared to previous Dilatometer studies. High rate charging led to capacity loss and irrecoverable material expansion.	Expansion was not dependent on discharge rate. The expansion followed a similar SOC dependence as Sample A at low SOC, but remained saturated during top of charge region. This could be explained by excess anode capacity of hand stacked cell.

Note also here that the expansion of the battery layers also has important consequences for quantification of the changes in lithium concentration during cycling of the battery. The change in neutron transmission between the charged and discharged states of the battery can be seen by comparing the line profiles shown in Figure 5. The increase in lithium concentration in the negative electrode (graphite) during charging leads to a decrease in neutron transmission. The change in local number of counted neutrons between two different images can be related to the change in local lithium concentration, c_{Li}, using the Beer-Lambert Law by assuming that the other material concentrations remain constant.[7] The shift in location of electrode layers prevents direct calculation of the change in lithium concentration. Therefore very accurate measurement of the expansion was needed to correctly re-align the battery layers to quantify the change in lithium concentration across each electrode as described in.[7] The change in lithium concentration across each of the 21 electrodes observed from neutron imaging is consistent with Coulomb counting and can be compared with the spatial distributions predicted by electrochemical models.[7]

Experimental Results

A summary of the experimental results is presented in Table II. Two pouch cells with similar materials and construction were used for the experiment. Sample A (the larger 120 mAh pouch cell) was taped onto a rigid mounting plate while Sample B was held under mild compression using a spring loaded fixture. Both cells were mounted on one side against a fixed aluminum block and free to swell toward the opposite side. Sample A was mounted on the right and Sample B was mounted on the left. The position of the battery in front of the detector was similar to the fixture used for Sample B (the 64 mAh pouch cell) as shown in Figure 1.

The expansion of each battery layer was measured using the peak localization algorithm described in the previous section. The mean and variance of the measurements along the y-axis are represented by the error bars shown in Figure 8, Figure 9, and Figure 10. The measurement variance for sample A, shown in Figure 8, is much less than for sample B shown in Figure 9. There are two sources of this variance; measurement uncertainty in the peak localization and variance in the actual material thickness. We propose two possible hypothesis for this difference in variance between samples A and B: 1) there is less variance in the material thickness for Sample A; 2) the wider electrode used for sample A actually has more well defined edges which causes less variance in the estimate of a_3 in Eq. 2. Note that the thickness of sample B was optimized for signal to noise ratio of lithium concentration change, not edge detection.

Relationship between negative electrode lithium stoichiometry and expansion.— For test A1, sample A was cycled at the C/5 rate for 2.5 hours then allowed to rest at 50% SOC for 2.5 hours before charging to 100% SOC with a constant voltage hold at 3.6 V until the current tapered off to C/100. The discharge process mirrored the charging profile for test A1, as shown in Figure 7. Figure 8 shows that the battery expanded linearly as a function of SOC up until SOC = 0.3 Between 0.3 and 0.7 SOC the expansion remained saturated with further charging. Finally for SOC values higer than 0.7 the expansion continuted until the battery was fully charged. Upon discharging, the battery thickness followed the same SOC dependence with a saturation in the middle region of SOC. However, it returned to a slightly compressed state relative to the initial relaxed value.

This expansion is consistent with the previous findings for lithium intercalation into graphite (see Figure 1a in[1] which found that a correlation between the voltage plateaus and expansion in graphite). The plateaus in the voltage profile, shown in the upper subplot of Figure 8, can be attributed solely to the negative electrode since the LiFePO4 has a very flat OCV curve. Therefore, the observed voltage plateaus correspond to lithium staging in the graphite described in.[1,12,13] The specific voltage profile of the intercalation staging depends on the type of carbon as shown in Figure 3 of,[14] and can be measured using half cells vs lithium metal reference electrode. In general, intercalation stage 1 correspond to 0–90 mV (at Vcell = 3.36 V, between 0.8 to 0.9 SOC), stage 2 correspond to 90–120 mV (at Vcell = 3.31 V between 0.4 and 0.6 SOC), stage 3 correspond to 120–210 mV (Vcell = 3.21 V near 0.1 SOC), and stage 4 correspond to >210 mV. The disappearance of the voltage plateaus at high C-rate, shown in the inset of Figure 6, is indicative that uniform staging across the electrode did not occur for our experiments at higher charging rates.

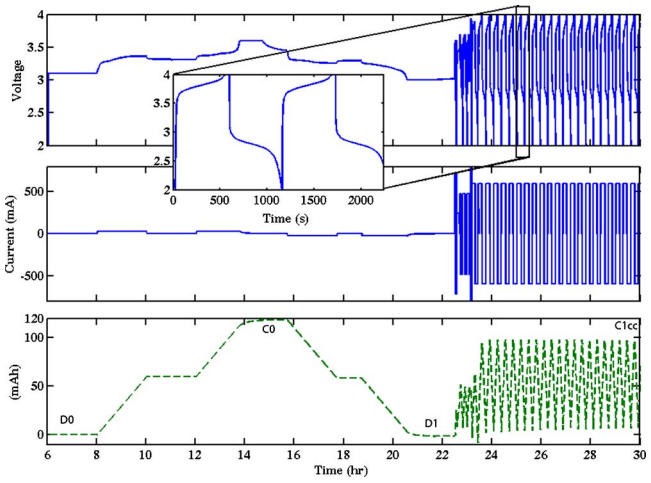

Figure 7. Measured voltage (top), applied current (middle), and stored charge (bottom) for the slow and fast cycling of Sample A. At the 5C rate approximately 75% of the total capacity was available when cycling between 2 and 4 V.

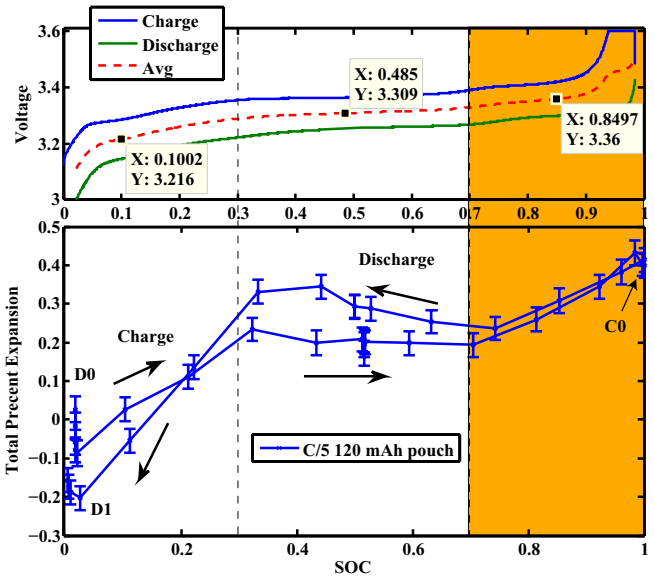

Figure 8. The upper subplot shows the battery voltage as a function of state of charge for test A1, the C/5 charge and discharge cycle. The percent expansion for Sample A at the C/5 rate is shown in the lower subplot. The error bars denote the variance in expansion along the y-axis. Saturation of the expansion occurs between 0.3 and 0.7 SOC corresponding to the staging of lithium within the graphite structure.

The upper subplot of Figure 9 shows the near Open Circuit Voltage (OCV) profile of sample B as a function of SOC for a C/20 cycle. In the lower subplot the expansion of the electrode as a function of SOC during tests B1 and B2 are shown. Two different stroboscopic profiles were applied to sample B. Test B1 consisted of 1C charge and 2C discharge cycling which was performed over the 2–3.6 V window as shown in Figure 3. Test B2 consisted of a 1C charge followed by a CV hold at 3.6 volt, and then the battery was discharged at the 5C rate for 180 s until the battery reached 0.5 SOC. The battery was allowed

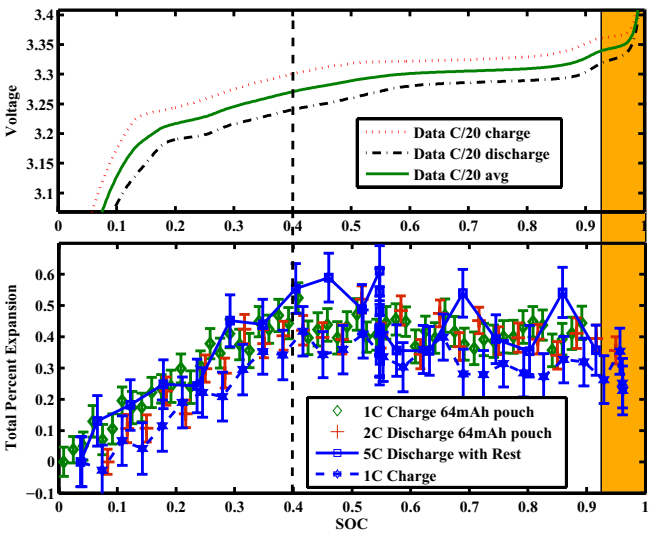

Figure 9. Lithium iron phosphate battery voltage versus state of charge at the 20 hour rate is shown in the upper subplot. The voltage range in the plot is cropped to illustrate the plateaus. In the lower subplot the percent expansion of the total battery for sample B is shown also as a function of SOC. The thickness of the battery varies linearly with SOC below 0.4 and is saturated above. Experiments with sample B show that the percent expansion was independent of the discharge current rate for values less than 5C.

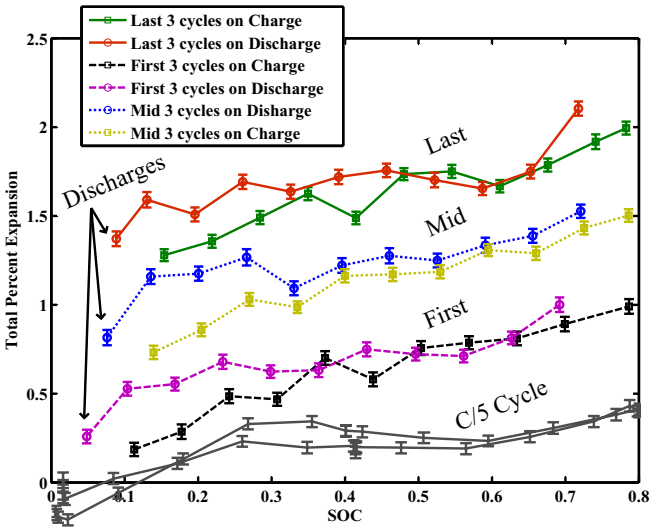

Figure 10. Percent expansion for Sample A observed during an experiment with high charge rate (5C) and expanded voltage operating window (2–4 V). During this high-rate cycling the battery was not allowed to rest between charge and discharge as shown in Figure 6. The expansion during C/5 cycling is also shown for comparison.

to rest for 180 s before discharging the rest of the way to 2 V at the 5C rate.

The battery percent expansion follows the same SOC dependence for tests B1 and B2, as shown in Figure 9; however it is different than that of sample A. In this case the battery thickness increased linearly with SOC, up to 0.4 SOC and above 0.4 SOC there was no further expansion. For sample B, the transition to the higher voltage plateau, corresponding to the highlighted region in Figure 9, occurs near 0.9 SOC instead of 0.7 SOC as observed for Sample A.

A difference in the relative anode capacity between sample A and B could explain the observed differences in the expansion as a function of state of charge. Previous dilatometer experiments have shown that the graphite expansion is a linear function of stoichiometry x in Li_xC_6 up to $x = 0.3$ with a saturation until $x = 0.7$ followed by further linear increase.[1] If we assume that the negative electrode of sample B has 30% excess capacity relative to the positive electrode active material, then 0.4 SOC corresponds to $x = 0.3$. These experimental observations are in agreement with prior results.[13,12] The typical anode excess capacity used in commercial cells can be as high as 20%. The capacity mis-match would also explain the shift in location of the start of the 2nd voltage plateau from 0.7 to 0.9 SOC; compare the highlighted regions of Figure 8 and Figure 9.

The measured 0.5% expansion of the total battery thickness corresponds to 1.7% of the active material thickness in the negative electrode, since the negative electrode's active material is 29.4% of the total thickness. This expansion is less than the 4% reported by Hahn et al.[1] for carbon, however the type of graphite and binder strength impact the electrode expansion. Additionally, the total battery expansion is the sum of the iron phosphate contraction and carbon expansion upon charging.[6] Therefore, if the $LiFePO_4$ is contracting at the same time, then the LiC_6 expansion could be even larger than what was inferred from the measurements. Unfortunately, we cannot determine the relative expansion of the positive and negative electrodes because the separator interface is not resolved in the line profile data from neutron imaging.

The effect of charging rate.— The effect of charging rate was investigated in a subsequent test (A2). Starting at t = 84,000 s sample A was cycled between 2 V and 4 V at the 5C rate as shown in Figure 6. A larger voltage window was needed to get resonable capacity when cycling of the battery at this high rate due to its large internal resistance. Eleven images, with 45s exposure time, were acquired during each

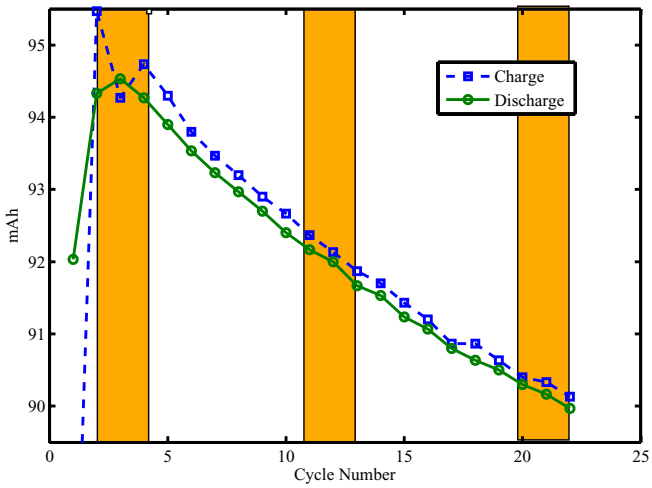

Figure 11. A 3% capacity loss occurred over the 21 cycles of 5C charging and discharging of sample A. The percent expansion of the first, middle and last 3 cycles are shown in Figure 10.

charge and each discharge period. The first image from each discharge cycle was averaged together to generate a stroboscopic snapshot of the battery (at 0.7 SOC). Similarly each of the other images were averaged across the 22 cycles to generate snapshots of the expansion at various SOC. At this high rate we observed a large offest in expansion at 0 SOC, as shown in Figure 11, relative to the relaxed case. We suspect that this was caused by the combination of high-rate and lack of relaxation period between charging and discharging, since the

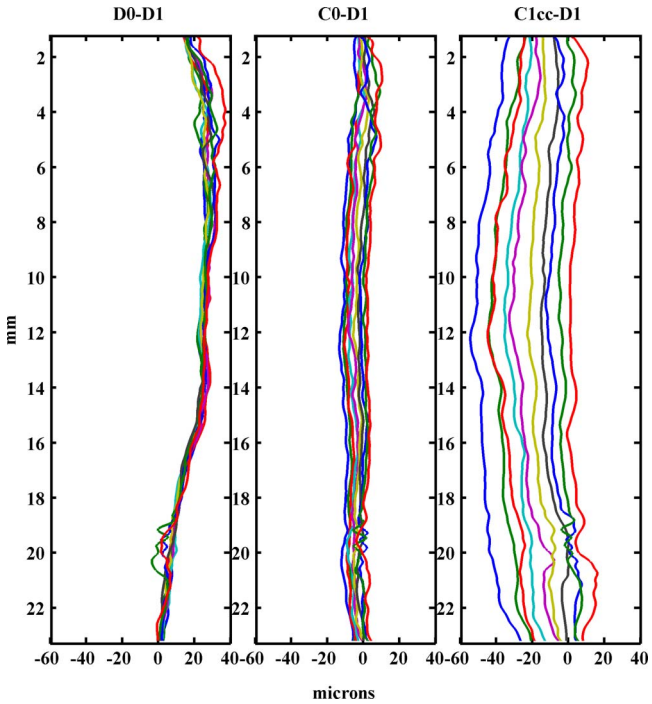

Figure 12. Displacements of the 10 peaks corresponding to the aluminum current collectors relative to the discharged state (D1), as indicated by the arrows in Figure 6. Subfigure (a) shows that the initial discharged state the battery was deformed, by curving along the y-axis and it became straighter during charging. The displacements of the aluminum layers are near zero indicating that the battery returned to same thickness in the discharged state. Subfigure (b) shows the normal expansion during charging. Subfigure (c) shows the abnormally large expansion in the charged state following the high rate cycling over an expanded voltage window.

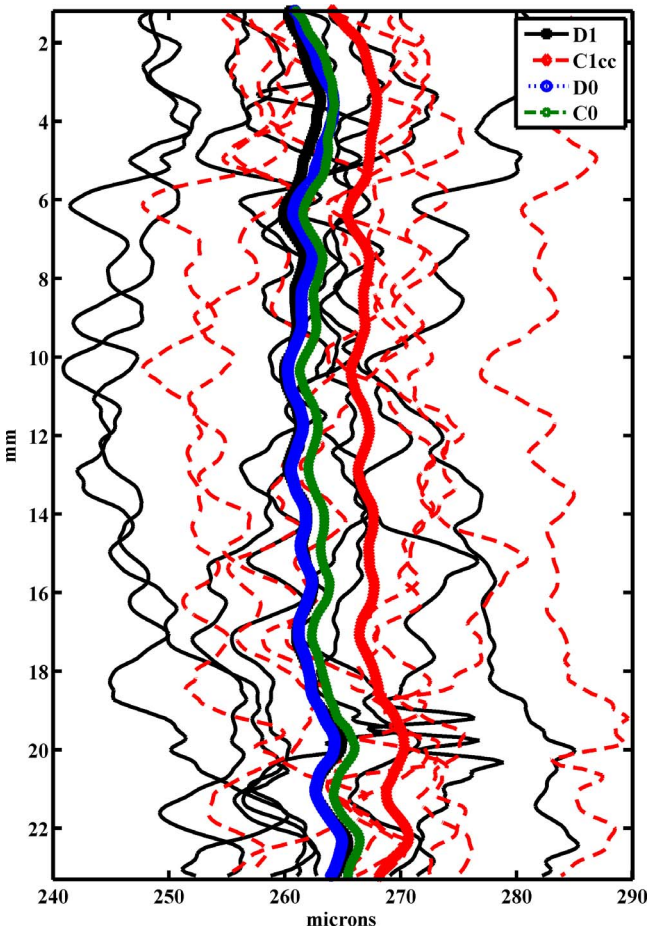

Figure 13. Thickness of the battery layers for Sample A in the charged and discharged states. The variance in thickness for each of the layers (9 peak to peak distances) for the D1 and C1cc cases are shown. The average thicknesses for all four cases are denoted by the thicker lines in the center of the figure.

opposite current was applied immediately upon reaching the voltage limit. A small linear increase in thickness with increasing SOC was observed across the entire cycle as compared to the saturating behavior observed at lower C-rates. Although some temperature rise (10–15°C) was expected during the 5C cycling the thermal expansion is on the order $\sim 10^{-5}$ m/m C or about 0.01% and should not contribute a measureable amount.

The number of Ah processed though the cell was tracked during the 5C cycling of the battery and a 4% decrease in cell capacity was observed as indicated in Figure 11. The decrease in capacity appears to be correlated with the cycle to cycle growth in battery thickness as shown in Figure 10, where the average expansion of the first three, middle three, and last three cycles are shown as a function of SOC. Note that sample B was discharged at the 5C rate, and charged at the 1C rate, but did not exhibit any permanent expansion or degradation in capacity throughout the experiment. Hence, the irreversible expansion observed in A2 may be related to lithium plating during high charging rate or overcharge (4 V) that can cause electrolyte and/or electrode decomposition.[15]

Uniformity of expansion.— The uniformity of the expansion along the length of the cell (y-axis) can also be investigated using NI. The location of each of the 10 aluminum current collectors for sample A is shown in Figure 6. The two sets of peaks, associated with the aluminum current collectors, correspond to the discharged state at the beginning (D0) and the charged state after high c-rate cycling (C1cc). The displacement, which is the separation between each pair of lines in Figure 6 and hence the expansion, of the layers is shown in

Figure 12. The battery initially had some curvature along the y-axis as a result of handling the cell. During charging at the beginning of experiment A1, shown in Figure 7, the battery layers became straighter. Subfigure (a) shows the difference in curvature of the electrode layers between the initial (D0) and 2nd discharge (D1) states. The displacement of the rightmost line indicates curvature of the entire battery structure relative to the reference state (D1). Following the C/5 charge and discharge the battery returned to its nominal thickness, observed by the clustering of the lines. Subfigure (b) shows the displacement of each layer corresponding to the normal expansion of the battery in the charged state, (following a C/5 charge) relative to the discharged state (D1). Figure 12c shows the larger expansion in the charged state following the 5C cycling over the wider voltage window. The non-uniformity of expansion along the y-axis is also visible in this figure, where the largest expansion is observed in the middle region along the y-axis and smallest at the ends. Figure 13 show the uniformity of the electrode thickness for each of the 10 layers.

Conclusions

The expansion of two lithium iron phosphate pouch cells has been observed via post processing of neutron images acquired during galvanostatic cycling. Sub-pixel resolution of features in the image is achieved by fitting a symmetric function to line profile data in order to measure the expansion. For sample B, the observed expansion was independent of discharging rate and demonstrated a saturation type behavior for SOC greater than 40% with no further expansion observed at higher SOC. The difference in transition points at low current cycling rate for the expansion vs. SOC relationship between samples A and B could be explained by the difference in anode excess capacity. The 0.5% expansion of the battery layers was attributed to lithium intercalation in the negative (graphite) electrode, which follows the staging of lithium in the graphite material.[12,13] The observed expansion agrees with previously published dilatometer and X-ray diffraction measurements of lithium batteries.

Both pouch cells showed similar traces of expansion vs. SOC at low C-rates, independent of the applied light compression. However, during high C-rate (5C) charging Sample A exhibited a 4% decrease in capacity that was correlated with an irreversible expansion relative to the relaxed state. The relationship between expansion and SOC at higher charging rate was also different. A linear increase in thickness across the entire range of SOC was observed as opposed to the saturation in the middle range of SOC, which indicates uniform lithium staging across the graphite electrode.

The advantage of NI over traditional methods for measuring expansion is that the spatial distribution, along the y-axis, can also be measured as opposed to a point to point measurement. In addition, the layer to layer variability can be investigated in pouch cells with multiple stacked electrodes because the location of each aluminum current collector is resolved. The largest expansion was observed near the center of the cell indicating that the pouch structure has some impact on the local expansion. The flatness of the electrode layers and spatial resolution of the detector currently limit the accuracy of the proposed method, however thicker electrodes or advances in the detector technology could improve the spatial resolution and allow us locate the separator which would enable differentiation between anode and cathode expansion. Future work is needed to investigate high-rate charging under compression to determine the impact of compression and charging rate on expansion.

Acknowledgments

The authors acknowledge Tracy Chin (formerly of A123 Systems) and William Hicks of Navitas Systems ASG for preparing the electrodes and assembling and forming the cells.

References

1. M. Hahn, H. Buqa, P. W. Ruch, D. Goers, M. E. Spahr, J. Ufheil, P. Novak, and R. Kotz, *Electrochem. Solid-State Lett.*, **11**(9), A151 (2008).
2. M. Winter, G. H. Wrodnigg, J. O. Besenhard, W. Biberacher, and P. Novak, *J. Electrochem. Soc.*, **147**(7), 2427 (2000).
3. K. Zhao, M. Pharr, J. J. Vlassak, and Z. Suo, *J. Appl. Phys.*, **108**, 073517 (2010).
4. J. H. Lee, H. M. Lee, and S. Ahn, *J. Power Sources*, **119–121**(0), 833 (2003).
5. Y. Zhu and C. Wang, *J. Power Sources*, **196**(3), 1442 (2011).
6. A. Yamada, S. C. Chung, and K. Hinokuma, *J. Electrochem. Soc.*, **148**, A224 (2001).
7. J. B. Siegel, X. Lin, A. G. Stefanopoulou, D. S. Hussey, D. L. Jacobson, and D. Gorsich, *J. Electrochem. Soc.*, **158**(5), A523 (2011).
8. D. S. Hussey, D. L. Jacobson, M. Arif, K. J. Coakley, and D. F. Vecchia, *J. Fuel Cell Sci. Technol.*, **7**(2), 021024 (2010).
9. C. Peabody and C. B. Arnold, *Journal of Power Sources*, **196**, 8147 (2011).
10. T. F. Coleman and Y. Li, *SIAM J. Optimization*, **6**, 418 (1996).
11. A. Harms and D. Wyman, *Mathematics and Physics of Neutron Radiography*, Springer (1986).
12. J. R. Dahn, *Phys. Rev. B*, **44**(17), 9170 (1991).
13. N. Takami, A. Satoh, M. Hara, and T. Ohsaki, *J. Electrochem. Soc.*, **142**(2), 371 (1995).
14. Y. F. Reynier, R. Yazami, and B. Fultz, *J. Electrochem. Soc.*, **151**(3), A422 (2004).
15. R. V. Bugga and M. C. Smart, *ECS Transactions*, **25**(36), 241 (2010).